TA●, Vol.7, N●.1, 61-82, March 1996

Further Studies of a Prefrontal Convective Rainband During TAMEX IOP 13: Part I: Reflectivity History and Cell Evolution

YEONG-JER LIN[1], ROBERT W. PASKEN[1], JOE G. ZILKA[1] and MARTIN R. MARTINO[1,2]

(Manuscript received 30 March 1995, in final form 22 January 1996)

ABSTRACT

Radar measurements obtained from both conventional and Doppler radars were used to study the life cycle of a prefrontal convective rainband during TAMEX IOP 13 on 25 June 1987. The conventional radar data were available at 20-min intervals, while Doppler data were available at 7-min intervals. Additionally, surface observations at 30-min intervals taken from nine stations over the west coast and the Taiwan Strait were also used for analysis to determine the approximate positions of the Mei-Yu front and the leading edge of the rainband (gust front).

Results show that a prefrontal convective rainband formed in the vicinity of the Mei-Yu front when the system was located far north of the island. As the rainband moved slowly down the central west coast, it began to move away from the front as gust fronts were formed by cells at the leading edge of the system.

The convective cells generated low-level cold outflows in the warm sector to the southeast of the front. Part of these cold outflows moved toward the southeast, interacting with the strong moisture-rich southwest monsoon flow to form a gust front. At the same time, the southwestern portion of the front, located 50-60 km west of the coast, continued to lift moist air, generating a new cell along the front. This new cell then traveled to the east at a more rapid speed following the prevailing westerly flow at low levels. It eventually merged with the main (old) cell, thereby prolonging the lifetime of the rainband. The analysis in this study, as a whole, further supports the conceptual model of this rainband reported in the study by Lin *et al.* (1992) using two volumes of dual-Doppler data obtained from CP-4 and TOGA (Tropical Ocean and Global Atmosphere).

(Key words: TAMEX, Long-lived rainband, Radar meteorology, Meso-meteorology)

[1] Department of Earth and Atmospheric Sciences, Saint Louis University, St. Louis, MO 63103 U.S.A.

[2] Present affiliation: The Air Weather Service, U. S. Air Force, U.S.A.

1. INTRODUCTION

In the studies by Lin *et al.* (1992) and Lin *et al.* (1993), the structure of a subtropical prefrontal rainband in the Taiwan Area Mesoscale Experiment (TAMEX) IOP 13 was investigated in detail using dual-Doppler data at 0653 and 0700 LST (local standard time), 25 June 1987. This convective rainband developed on the warm side of a Mei-Yu front over northwestern Taiwan as the front was approaching the northwest coast. The front retained its baroclinic character before reaching the central and southern portions of Taiwan. The cold pool behind the Mei-Yu front mechanically lifted the warm, moist strong southwest monsoon flow in the boundary layer. The lifted parcel became saturated near 1 km. In the absence of mixing with the environment, this parcel (after about 100 mb of lifting) became positively buoyant and ascended freely above 200 mb. Hence, organized convection was initiated and maintained by the frontal lifting of a low-level jet (LLJ) in the boundary layer, and the main moisture supply came from the high-θ_e monsoon air at low levels. The rainband formed in the vicinity of the Mei-Yu front in the earlier stage of the rainband's life cycle when the system was located far north of the island.

As the system moved down the central west coast of Taiwan, the rainband gradually intensified and became more organized. Composed of many cells, each one was accompanied by a moderate convective updraft (6-8 m/s) and a weak convective downdraft (2-4 m/s). As the updraft air reached 5 km and higher, it reversed its direction and merged with the northwesterly flow in the middle and upper troposphere. As a result, the reflectivity core was elongated toward the southeast with the environmental shear vector. This elongated reflectivity core induced the convective downdraft on the warm side of the front due largely to precipitation loading. Consequently, a distinctive convective rainband formed in a broad area ahead of the Mei-Yu front. During the mature stage of the rainband's life cycle, the rainband was 5-10 km wide and 100-120 km long. It moved slowly along the central west coast toward the south-southeast at 2.5 m/s. The maintenance of this long-lived rainband was caused by the factors of 1) frontal lifting; 2) a gust front arising from the convective downdraft ahead of the front; and 3) discrete developments in advance of the line. For more details, see Figure 25 and Section 5e in Lin *et al.* (1992).

The observational evidence presented in the current study further confirms that the frontal lifting did play an important role in the initiation and maintenance of the rainband in the earlier stage of the rainband's life cycle. However, the Mei-Yu front gradually lost its direct influence on the rainband in the area near the coastline as the system moved down the central west coast of Taiwan. During that period, the rainband began to move away from the front as gust fronts were formed by cells at the leading edge of the system. The convective cells generated low-level cold outflows in the warm sector to the southeast of the front. Part of these cold outflows moved toward the southeast, interacting with the strong high-θ_e southwest monsoon flow to form a gust front in the warm sector ahead of the front. As a result, new cells developed along the gust front. At the same time, the southwestern portion of the front, approximately 50-60 km west of the coast, continued to lift moisture-rich air on the warm side of the front, generating new cells along the front. These new cells then traveled to the east at a more rapid speed following the prevailing westerly flow at low levels. They then merged with the old cells, thereby prolonging the lifetime of the rainband. The density-current mechanism resulting from the cold outflows of convective cells in the lower layer was likely to be responsible for the more rapid movement of the rainband than the slow movement of the Mei-Yu front. The slow movement of the cold front during the

IOP 13 was, in part, attributed to the relatively weak northwesterly wind in the lower layer behind the front as evidenced in the 850 mb flow chart (see Figure 3a in Lin *et al.* 1992). Additionally, the effect of the Central Mountain Range (CMR) also played a role in slowing down the system movement; for example, see studies by Mannouji and Kurihara (1990), etc.

The purpose of this study in Part I is to provide additional observational evidence to support the conceptual model of a prefrontal convective rainband in IOP 13 presented in the study by Lin *et al.* (1992) described above. The kinematic structure of the rainband over a period of more than one hour as seen from the TOGA radar is presented in Part II of this study. In Part I, the surface traces obtained from nine stations over the west coast and the Taiwan Strait were employed to identify the positions of the cold front and the leading edge of a prefrontal convective rainband. Additionally, the reflectivity history of the rainband revealed by both the Kaohsiung and TOGA radars were used to demonstrate line motion, precipitation pattern, cell merger and other related features. Such structural features make it possible for researchers to further understand the formation and maintenance of this long-lasting, heavy-rain-producing convective rainband during the TAMEX IOP 13.

2. DATA AND METHODOLOGY

The data used in this study included the surface observations at 30-min intervals from 0200 to 2400 LST 25 June as well as radar observations obtained from the Kaohsiung (744) conventional radar, and the TOGA (770) Doppler radar. The conventional radar data were available at 20-min intervals, while the Doppler data were available at 7-min intervals. Temperature, dewpoint temperature, station pressure, significant weather, wind direction and speed along with the rainfall rate at each station were carefully analyzed to determine the approximate locations of the Mei-Yu front and the leading edge of the rainband.

As mentioned in Lin *et al.* (1992), the TOGA radar was unable to begin observation until 0653 LST 25 June. At the time of data collection, the radar site had already been surrounded by widespread convection. As a consequence, radar measurements were set at the VAD (velocity-azimuth display) mode, collecting data at 20 elevations. It took approximately 7-8 min to complete each volume scan. Eleven consecutive volume scans at 0653, 0701, 0708, 0716, 0724, 0732, 0740, 0747, 0755, 0802 and 0810 LST 25 June were employed in this study. These authors used NCAR's Research Data Support System (RDSS) to process raw Doppler data. Ground clutter was suppressed, and range and velocity foldings were eliminated. Only those data with high signal-to-noise ratio values were retained in the analysis. Since the intense convective regions were near the TOGA radar site at the times of analysis, the combined effects of earth curvature and attenuation on reflectivity were found to be very small.

3. DISCUSSION OF RESULTS

3.1 Surface Observations

The enhanced surface network began collecting data at 30-min intervals right after the IOP 13 commenced. With this volume of data available for analysis, several features of the Mei-Yu front and the associated rainband could be determined at a high confidence level in their accuracy. The time variations of surface observations at every 30 min obtained from nine stations over the northwestern and central west coast and the Taiwan Strait are presented

in Figure 13 of Lin (1993). In the figure, the passage times of the convective rainband gust front (GF) and cold front (F) are indicated. The positions of GF and F were subjectively determined based on the variations of surface parameters prior to, during, and after the passage of the system (see the following discussion for details). Typically, the passage of the prefrontal squall line was accompanied by signs of the GF with rising pressure, temporary cooling and temporary wind shifts. On the other hand, the passage of the Mei-Yu front was characterized by signs of steady pressure rise, temporary cooling and distinctive wind shifts from southwest to northeast.

Analyses of these surface observations reveal that the rainband was located very close to the front at the CAA (Civil Aeronautic Administration) radar site around 0300 to 0400 LST. As the frontal system moved slowly toward the south-southeast along the northwest coast of Taiwan, the rainband quickly moved away from the cold front. The leading edge of the rainband (GF) reached Tao-Yuan around 0400 LST, approximately 15 min ahead of the frontal passage. There was a rapid wind shift from southwesterly to northeasterly winds, and convective activity did not commence until after the passage of the cold front. Both temperature (T) and dewpoint temperature (T_d) decreased by nearly 5°C within three hours of the frontal passage. Pressure (P) rose steadily after frontal passage and increased nearly 4 mb. Dewpoint depression did not decrease until 6-8 h after the Mei-Yu front passed; thus, it took several hours for the low-θ_e air from northern China to arrive.

As the system continued to move down the coast, the rainband moved more rapidly away from the cold front. The GF passed Hsin-Chu at about 0415 LST, but the front did not pass until around 0830 LST, a 4 h difference from Tao-Yuan despite the close proximity of the two stations. The southwest flow was able to feed moisture-rich air along the GF, thus enabling convection to sustain itself for nearly three hours. Upon frontal passage, the wind shifted in a similar fashion to the Tao-Yuan station with there only being a gradual decrease of 3°C in T and T_d from the GF passage until 1 h after the frontal passage. However, it took 2 h after the frontal passage before the dewpoint depression dropped significantly (4-5°C).

Wu-Chi is located right along the coast and displays some interesting features. GF passage and the Mei-Yu front passage were nearly 15 h apart with convection lasting only a couple of hours. However, several reports of heavy rain after the convective activity ceased indicated substantial moisture advection into the system, thus enhancing heavy precipitation. Temperature, dewpoint temperature and pressure all maintained a quasi-steady observation until the frontal passage. The Ching-Chung-Kang (CCK) station, where the TOGA radar was located, is slightly farther inland then Wu-Chi. The GF passed at about 0745 LST with convective activity being reported for nearly six hours. Just as in Wu-Chi, the frontal passage was about 15 h after the GF passage. Persistent strong winds (about 10 m/s) obviously transported moist air into the convective area, enhancing the probability of new cells developing ahead of the front. At Tai-Chung, convection preceded the GF passage (at 0845 LST), but heavy rains were consistently reported for five hours, thus leading to the understanding that it was a slow movement with persistent rains and not the intensity of the convection itself (Lin *et al.* 1992) that led to the flash floods.

Looking at two coastal island stations over the strait, Peng-Hu and Tung-Chi-Tao, it is noticed that the GF passage and the Mei-Yu front passage were much closer together than at the central stations (only 4-5 h apart). Most likely the speed of the front was not influenced as much by the CMR in these locations. The lack of convective activity and the overall short duration of the precipitation should also be noted. Temperature, dewpoint temperature and pressure all remained steady throughout the passage of the system, indicating that the

southern portion of the front underwent more air mass modification than the other regions (Trier *et al.* 1990).

The aforementioned surface traces further reveal that high-θ_e air dominated before the frontal passage at most northern stations. The dewpoint depression reduced to nearly zero 1-4 h after the frontal passage, showing cool, saturated air near the surface. On the other hand, the dewpoint depression became larger several hours after the frontal passage, indicative of the dominance of low-θ_e air from northern China. The surface traces displayed all show that the passage of the prefrontal rainband was accompanied by signs of a gust front with temporary cooling and wind shifts.

A synopsis of 16 coastal stations is depicted in Table 1. The stations are displayed such that as you read down the table, you are heading south in a direction pertaining to the location of each station. It is interesting to note the time differential between the gust front and the Mei-Yu front passage between the northern and the central stations. The gust front progressed steadily southward along the west coast, while the cold front moved much more slowly. Table 1 also indicates that southwesterly winds dominated, thus enabling moist air to feed the system. Temperature changes were almost null after the GF passage over most of the central west coast stations. However, there was generally a 2-5°C drop in temperature after the front passed over the northwest coast. These surface traces clearly show that the frontal system modified its properties from more baroclinic to less baroclinic in behavior as it traveled slowly down the west coast.

3.2 Rainfall Distribution

The rainfall distributions (in 30-min intervals) in relation to the GF and F are presented in Figure 14 of Lin (1993). Notice that the frontal position (F) trailed the leading edge of the heavy precipitation by 3 h at Hsin-Chu by 14 h at Wu-Chi and by 15 h at Tai-Chung. In contrast, the rainband gust front (GF) passed through each station before the leading edge of the precipitation maximum. The heavy precipitation occurred 1-2 h after the passage of the GF, indicative of the prefrontal convective rainband. Among the five stations shown, CAA (686) and Tao-Yuan (697) received their heaviest amount of rainfall (30-50 mm) within one-and-a-half hours after the Mei-Yu front passed. However, these totals were small compared to those of the other stations.

Hsin-Chu (756) received 10-20 mm of rain every half hour from the time the gust front passed until one hour prior to the frontal passage. This totaled nearly 100 mm of rainfall within three and a half hours. Wu-Chi (777) reported approximately 80 mm of rainfall between the period of 0730-0900 LST. Moderate to heavy rain continued for several hours adding nearly 65 mm more to that total. The largest amount of rainfall was received by Tai-Chung (749) where convection was followed by five hours of heavy rain (about 170 mm). Between 0900 and 1100 LST alone, 80 mm was reported. Coupled with the drainage from the mountainous regions nearby, it is easy to understand why extensive flash flooding occurred in the central west coast region of Taiwan.

The 24-h accumulated rainfall distribution for 25 June over Taiwan is depicted in Figure 9 of Lin *et al.* (1992). The contour interval was 40 mm per 24 h. Two areas of up to 200 mm occurred near the TOGA radar with the northern and central west coast of Taiwan receiving the most rain.

Table 1. Surface observations obtained from several west coast stations and the stations over the Taiwan Strait during the IOP 13, showing, winds, pressure, temperature and significant weather. The approximate positions of the Mei-Yu front and the leading edge of the rainband (gust front) were subjectively determined from the surface traces.

Station Name	Station Code	Passage Time (LST)		Surface Traces during Squall Passage				
		Squall line (GF)	Mei-Yu front	Wind direction	Wind S (m/s)	Pressure (mb)	Temperature (°c)	Weather
Tan-Shui	46690	0345	—	SE-NE	1-3	01.2-01.9	24-24	...
CKS Airport (CAA)	686	0315	0330	SW-N	3-5	01.4-02.7	27-26	R
Tao-Yuan	697	0400	0415	SW-NE	2-5	99.9-00.7	26-26	R
Hsin-Chu (AF)	756	0415	0830	SW-W	5-3	00.8-01.9	27-27	R
Hsin-Chu	757	0445	0915	SSW-SW	2-3	00.7-01.6	27-26	R
CP-4	—	0530	1300	SW-W	—	—	—	R
CCK (TOGA)	770	0745	2300	SSW-W	4-7	04.0-04.8	26-26	R
Wu-Chi	777	0700	2145	SSW-SW	6-8	02.6-03.5	28-28	R
Tai-Chung	749	0845	—	SSW-SW	2-3	03.5-04.4	27-27	R
Ma-Kung	734	1300	1800	SSW-SW	5-6	03.0-03.6	27-27	R
Peng-Hu	735	1315	1815	SSW-WSW	5-6	03.0-03.3	27-27	R
Tung-Chi-Tao	730	1700	2200	SW-W	5-6	02.9-03.9	26-26	..
Chia-Yi (AF)	746	1615	—	S-SSW	2-3	03.7-03.8	28-28	R
Chia-Yi	748	1600	—	SSE-S	2-3	03.0-03.4	28-28	..
Tai-Nan	741	2200	—	WSW-S	2-3	05.0-05.2	27-27	..
Tai-Nan (AF)	743	2245	—	WSW-S	2-3	05.1-05.4	28-27	..

3.3 Conventional Radar Signatures

The 10-cm Kaohsiung radar reflectivity distributions during the IOP 13, in relation to the gust front (indicated by the heavy dashed line) and the Mei-Yu front (denoted by the heavy solid line), at the constant altitude (approximately 3 km above sea level) are shown in Figure 8 of Lin (1993). The CAPPI (constant altitude plan-position indicator) displays of reflectivity covered the period from 0300 to 1000 LST 25 June. As stated earlier, the gust front and Mei-Yu front locations were subjectively determined based on the surface observations discussed previously in Section 3.1. A similar plot without the gust front superimposed for the period from 0400 to 1100 LST can also be found in Figure 5 of Lin *et al.* (1992).

In summary, the precipitation signatures were located along and behind both the gust front and Mei-Yu front at 0300 LST. By 0400 LST, the signatures started to elongate in an east-northeast to west-southwest orientation ahead of the front with a cell located near the

CAA radar. By 0500 LST, a line of cells (constituting the first semblance of a prefrontal rainband) developed in the area between the gust front and Mei-Yu front. At 0600 LST, the gust front moved along the coast of west central Taiwan. Several stronger cells developed within the dual-Doppler coverage area and were again located ahead of the Mei-Yu front. By 0700 LST, a distinctive prefrontal rainband had developed along this coast. At this time, the rainband was located in the southeast corner of the dual-Doppler coverage area. By 0800 LST, the convective cells began to dissipate; however, a new line of cells appeared to be developing along the gust front from 0900 to 1000 LST. These new cells continued to grow over the next several hours, and perhaps a new gust front formed to the south of these cells due to their outflows. Unfortunately, these cells were outside the dual-Doppler coverage area. By 1800 LST, almost all convective activity had dissipated as the front pushed onto land, thus cutting off its source of moisture.

Figure 1a is reproduced from Figure 9 of Lin (1993) and shows the successive hourly positions of the squall-line leading edge (GF) as determined from the surface traces described above. The position of the Mei-Yu front at 2000 LST 24 June is also shown. For comparison, the corresponding positions of the cold front at 3-h intervals, adapted from the study by Jou and Deng (1990), are also shown (Figure 1b). Notice that the frontal position trailed the gust front by many hours as the system moved slowly down the central west coast.

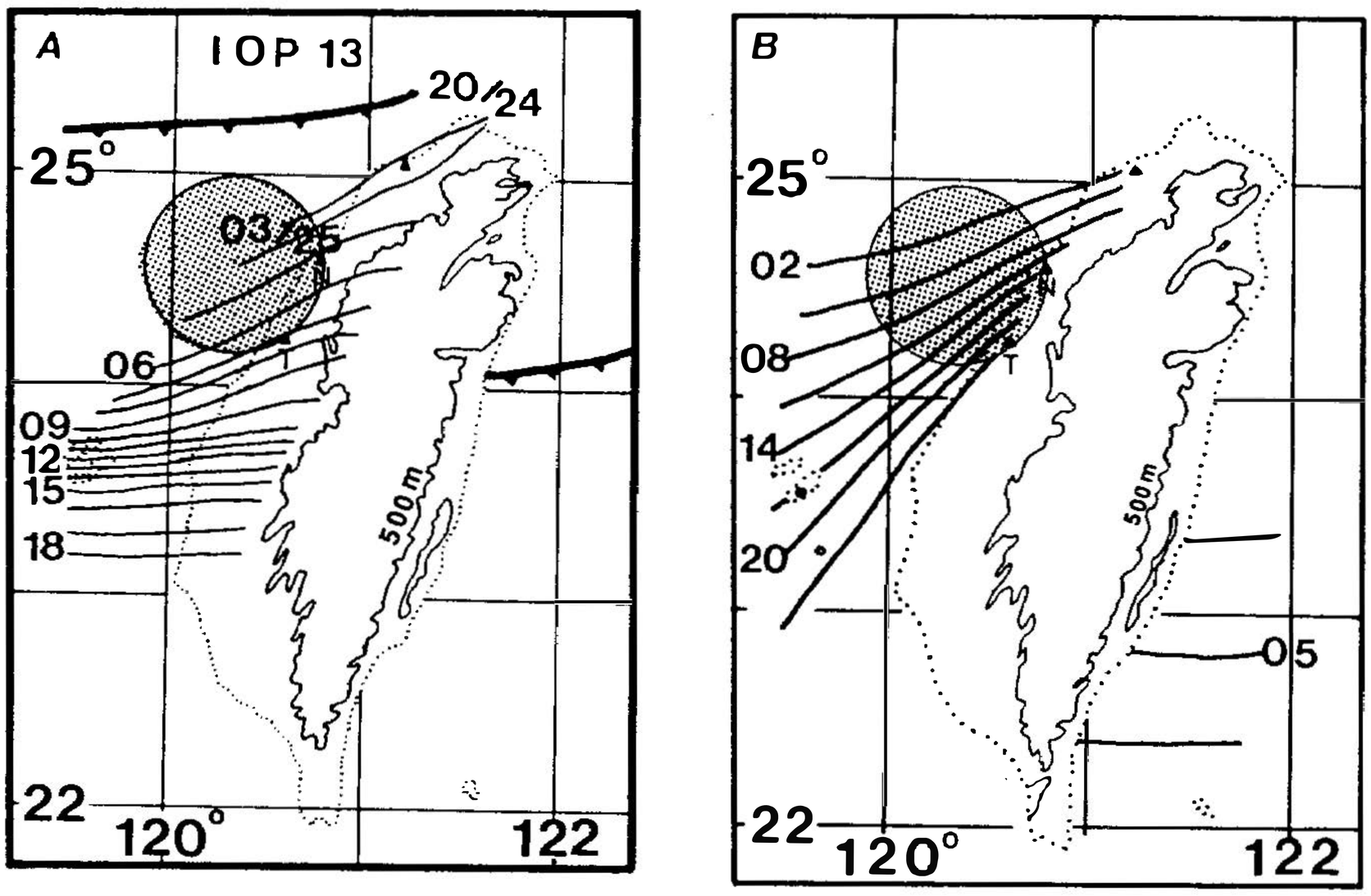

Fig. 1. The successive positions of (a) the squall-line leading edge in 1-h intervals, and (b) the surface cold front in 3-h intervals during the IOP 13 as determined from the surface data. Adapted from Lin (1993) and Jou and Deng (1990).

3.4 Doppler Radar Signatures

The reflectivity history of the rainband, as the system approached the central west coast of Taiwan, can be studied from the PPI displays of TOGA at low elevation angles. The 3° PPI scans for eleven successive times/occasions of analysis from 0653 to 0810 LST are

presented in Figures 2 and 3. The cold front has been superimposed on the first two volume scans from the dual-Doppler analysis results of Lin *et al.* (1992) and Lin *et al.* (1993). Notice a mesoscale wave-like pattern with a typical wavelength of about 15 km. Strong low-level winds across the front can produce small-scale vortices nearly 13 km along the gust front (Carbone 1982).

Inspection of Figures 2 and 3 reveals that the rainband had a more circular pattern than that of a typical squall line. This is attributed to the fact that the rainband observed in the IOP 13 was dominated by a strong northwesterly flow in the middle and upper layers, causing the convective cells along the cold front to be elongated toward the southeast. As a result, convective downdrafts formed in a broad area ahead of the front in the warm sector, due largely to precipitation loading (Lin *et al.*, 1992 and Lin *et al.*, 1993). It is seen that the width of the rainband (with reflectivities > 30 dBZ) was about 15-20 km. The rainband was oriented in a northeast-southwest direction. There were many cells embedded within the rainband. The maximum reflectivity was 45 dBZ.

A large area of high reflectivities (Z > 30 dBZ) was located to the northwest of TOGA. This convective region was mainly responsible for the heavy precipitation reported at Wu-Chi and CCK in the period from 0700 to 0800 LST. It is seen that the frontal system moved very slowly toward the south-southeast, traveling at a speed of only 2 m/s over a period of about 80 min. It is shown later that the front became almost stationary after 0716 LST as it was approaching the coastline. Also evident was a weak stratiform precipitation behind the front. Weak echoes (Z <15 dBZ) were observed beyond the 60 km range, but they advanced to within 40 km by the final scan.

3.5 Cell Merger

The conceptual model of this rainband, based on the dual-Doppler data obtained from the CP-4 and TOGA radars at 0653 and 0700 LST 25 June, is presented in Lin *et al.* (1992) (their Figure 25). The rainband developed on the warm side of the front over northwestern Taiwan as the Mei-Yu front was approaching the northwest coast. The front provided lifting which initiated the convection along the cold front. It traveled slowly at 2.5 m/s from the north-northwest due to the relatively weak environmental wind (only 4-5 m/s from the northwest) in the lower layer. The rainband was about 100 km long and was composed of many cells each of which was accompanied by a moderate convective updraft and a weak convective downdraft. The descending air of this weak convective downdraft produced a horizontally diverging flow in the boundary layer. Part of this cool diverging flow moved southeastward, interacting with the incoming high-θ_e environmental air to form a gust front in the warm sector. As a result, new cells developed ahead of the GF. These new cells moved toward the east and northeast at a speed faster than the system speed following the prevailing flow at low levels. These cells eventually merged with the main (old) cells near the west coast, thereby prolonging the life span of the rainband.

Figure 4 is the PPI display of reflectivity for the lowest elevation (0.3 degree). This display presents an excellent example of cell merger illustrating how a new cell, located to the west of the main cell, merged with it during a time span of 46 min. This new cell, identified as cell A in the figure, apparently formed before 0653 LST over the southwestern edge of the rainband. It was observed about 35 km west of TOGA at 0653 LST (Figure 4a) and moved toward the east at approximately 7 m/s following the westerly wind in the lower layer. In contrast, the main cell, located to the northwest of TOGA, traveled very slowly at

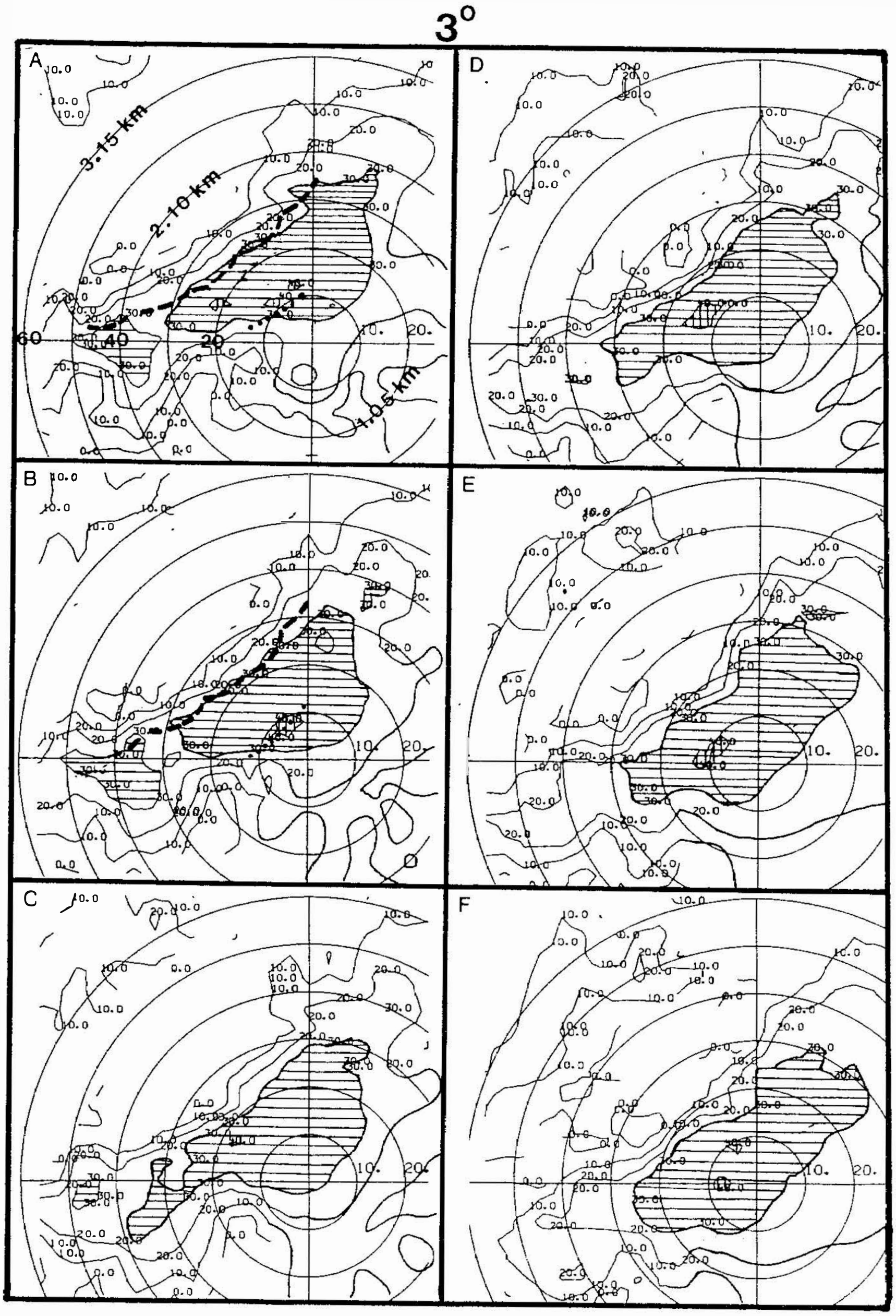

Fig. 2. PPI reflectivity (Z) displays at 3 degree elevation as seen from the TOGA Doppler radar for (a) 0653, (b) 0701, (c) 0708, (d) 0716, (e) 0724, and (f) 0732 LST 25 June. The contour interval is 10 dBZ. The approximate positions of the Mei-Yu front and gust front at 0653 and 0701 LST, as determined from dual-Doppler analyses by Lin et al. (1992) and Lin et al. (1993), are superimposed. Heights at 20, 40, and 60 km from TOGA are indicated in panel a. Areas with $Z > 30$ dBZ are hatched.

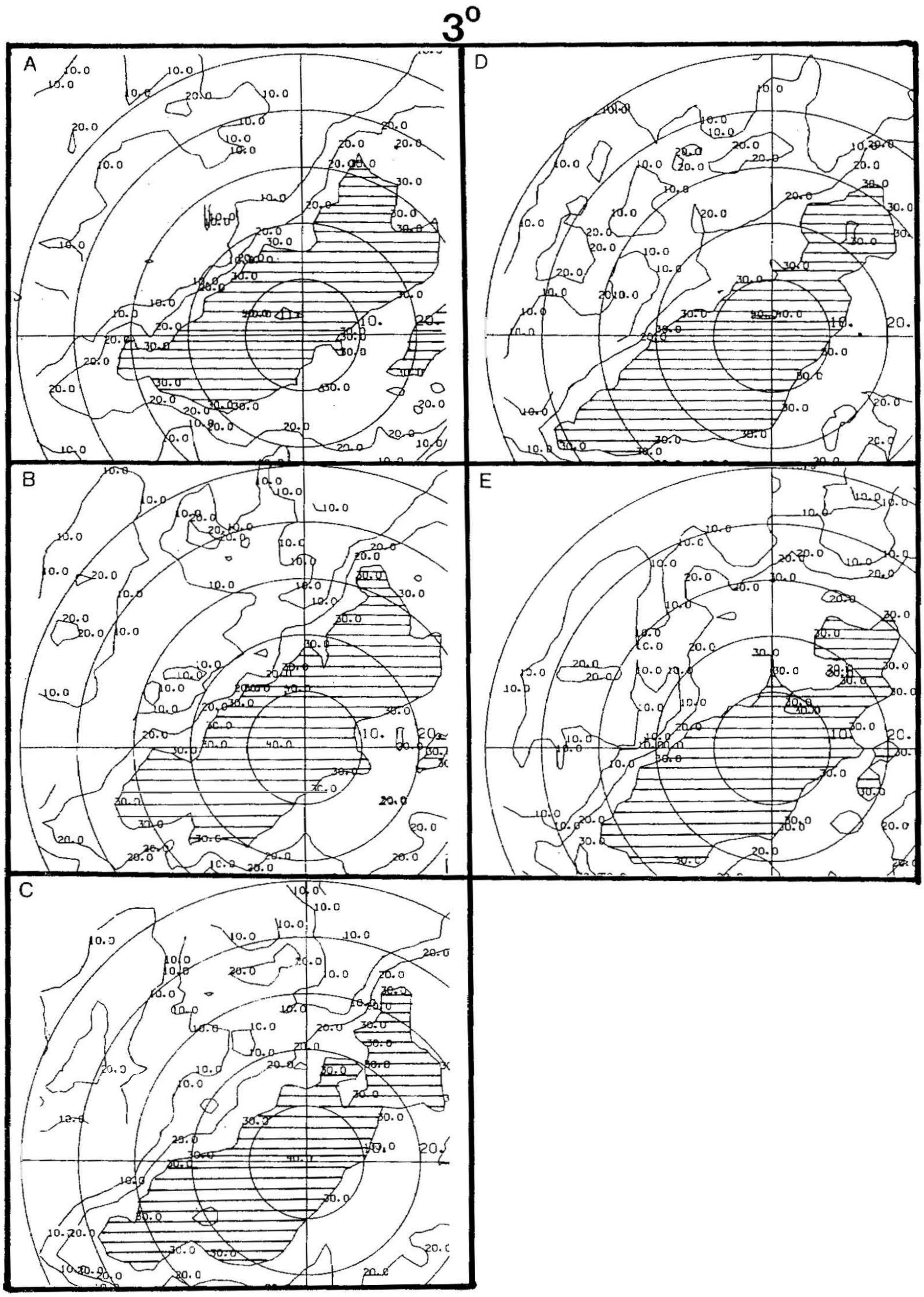

Fig. 3. As in Figure 2 except for (a) 0740, (b) 0747, (c) 0755, (d) 0802, and (e) 0810 LST 25 June.

2-3 m/s toward the south-southeast (Figures 4b-4d). Cell A reached the southwestern edge of the main cell around 0724 LST (Figure 4e) and eventually merged with the main cell after 0732 LST (Figure 4f). A similar feature of cell merger, but for the earlier time periods in the IOP 13, is also reported in the recent study by Li *et al.* (1995). This example, together with those surface features presented earlier, appear to provide further evidence to support the conceptual model presented in Lin *et al.* (1992). It strongly suggests that the leading edge of the convective rainband plays an important role in initiating a new cell as the low-level cold outflow, associated with the convective downdraft ahead of the Mei-Yu front, interacts with the high-θ_e southwest monsoon flow in the warm sector. This mechanism continues to prevail until the system reaches the southwest coast of Taiwan.

3.6 RHI Display

The RHI (range-height indicator) slices of the rainband were not part of the scanning strategy. The RHIs were derived from the entire volume of vertically stacked PPI scans, with the objective analysis scheme developed at Saint Louis University (Pasken and Lin, 1991) being used. The azimuth angle chosen for investigation was nearly normal to the advancing rainband. Reflectivities and radial velocities were taken from the RHI slices, while the horizontal velocities were determined by geometry using range and height.

Radial velocities for six successive times of analysis along the 310 degree radial in a direction nearly perpendicular to the rainband are shown in Figure 5. Negative values indicate the flow toward TOGA, while positive velocities (hatched line) indicate the flow away from the radar. Contours are every 2 m/s with the Mei-Yu front represented by the heavy dashed line. The range is northwest of the radar above sea level.

At 0653 LST (Figure 5a), the front was located about 24 km northwest of TOGA. This was determined by the shift from negative to positive velocities, resulting in a maximum low-level convergence at the leading edge of the front. Note positive velocities ahead of the front were associated with the southwesterly winds in the warm sector, while negative values behind the front were associated with the westerly and northwesterly winds at low levels. The gust front , as reported in Lin *et al.* (1993), was located about 9-10 km northwest of TOGA and was characterized by weak convergence and slight wind shift. This gust front was related to the leading edge of the rainband as it moved slowly toward the TOGA radar. An area of -20 m/s in the upper levels was due to the high-level northwesterly flow, which was nearly parallel to the radar beam allowing for a nearly true indication of the velocity.

At 0701 LST (Figure 5b), both the GF and front had advanced 1-2 km toward the radar. There was also a region of strong mid-level flow between 6 and 12 km similar to that at 0653 LST. The front was located about 18.5 km from TOGA at 0708 LST (Figure 5c), while the GF was seen at 8 km, approximately 11 km southeast of the Mei-Yu front.

The cold front remained nearly stationary in the period between 0716 and 0732 LST (Figures 5d-5f). On the other hand, the GF continued to move slowly toward the radar site as indicated. In the middle and upper layers, the northwesterly wind dominated in a broad area between the GF and the front.

Figure 6 displays reflectivity along the same radial (310 degree) with contours every 5 dBZ. Areas with $Z > 40$ dBZ are hatched. Notice that a broad area of 35 dBZ or greater occurred in the region ahead of the front and extended to the radar site, indicative of the convective region. Conversely, reflectivities were weak in a shallow region behind the front corresponding to the stratiform region. These results show two types of precipitation in the

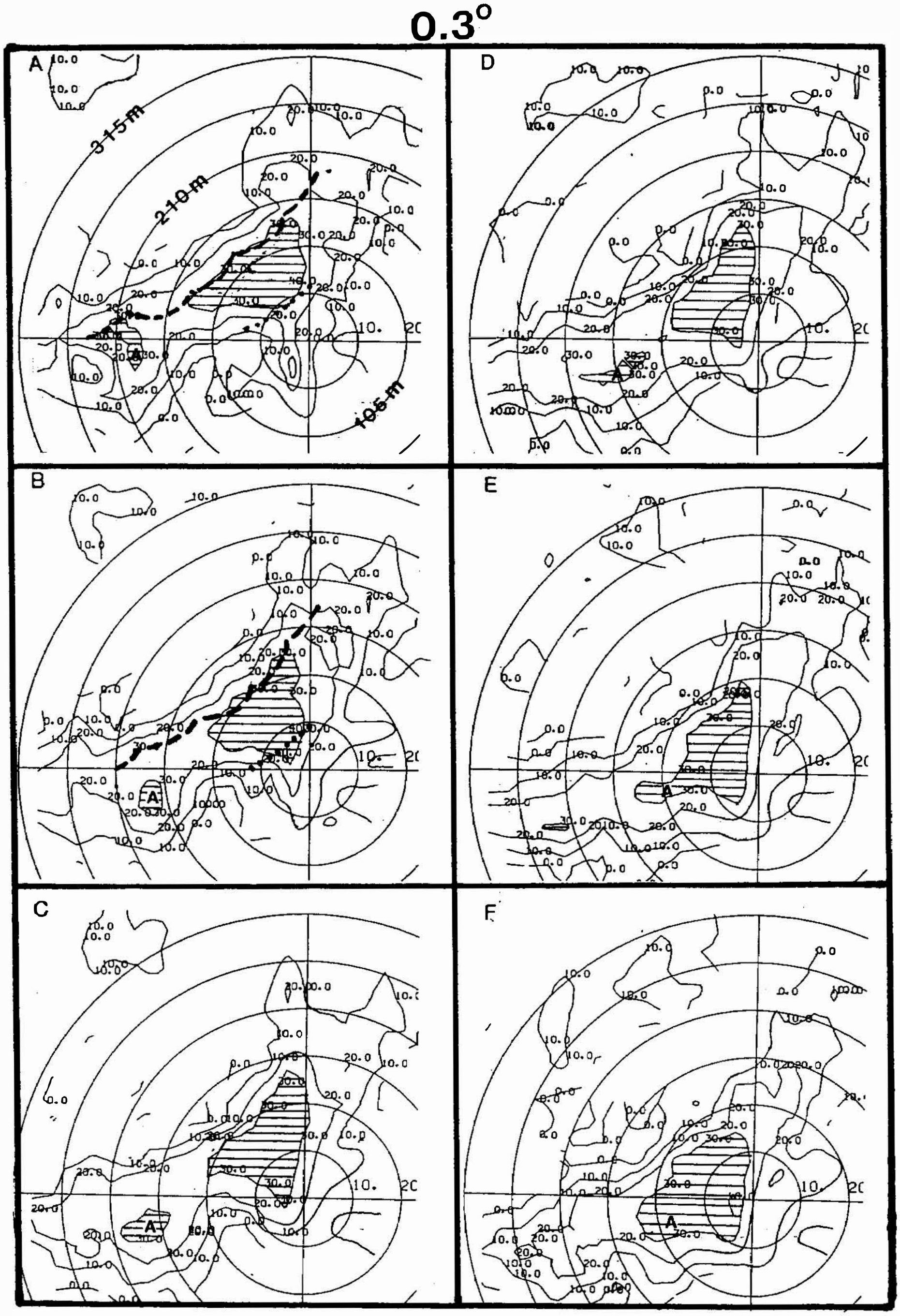

Fig. 4. PPI reflectivity (Z) displays at 0.3 degree elevation for (a) 0653, (b) 0701, (c) 0708, (d) 0716, (e) 0724, and (f) 0732 LST 25 June. Heights at 20, 40, and 60 km from TOGA are indicated in panel a. Areas with Z > 30 dBZ are hatched.

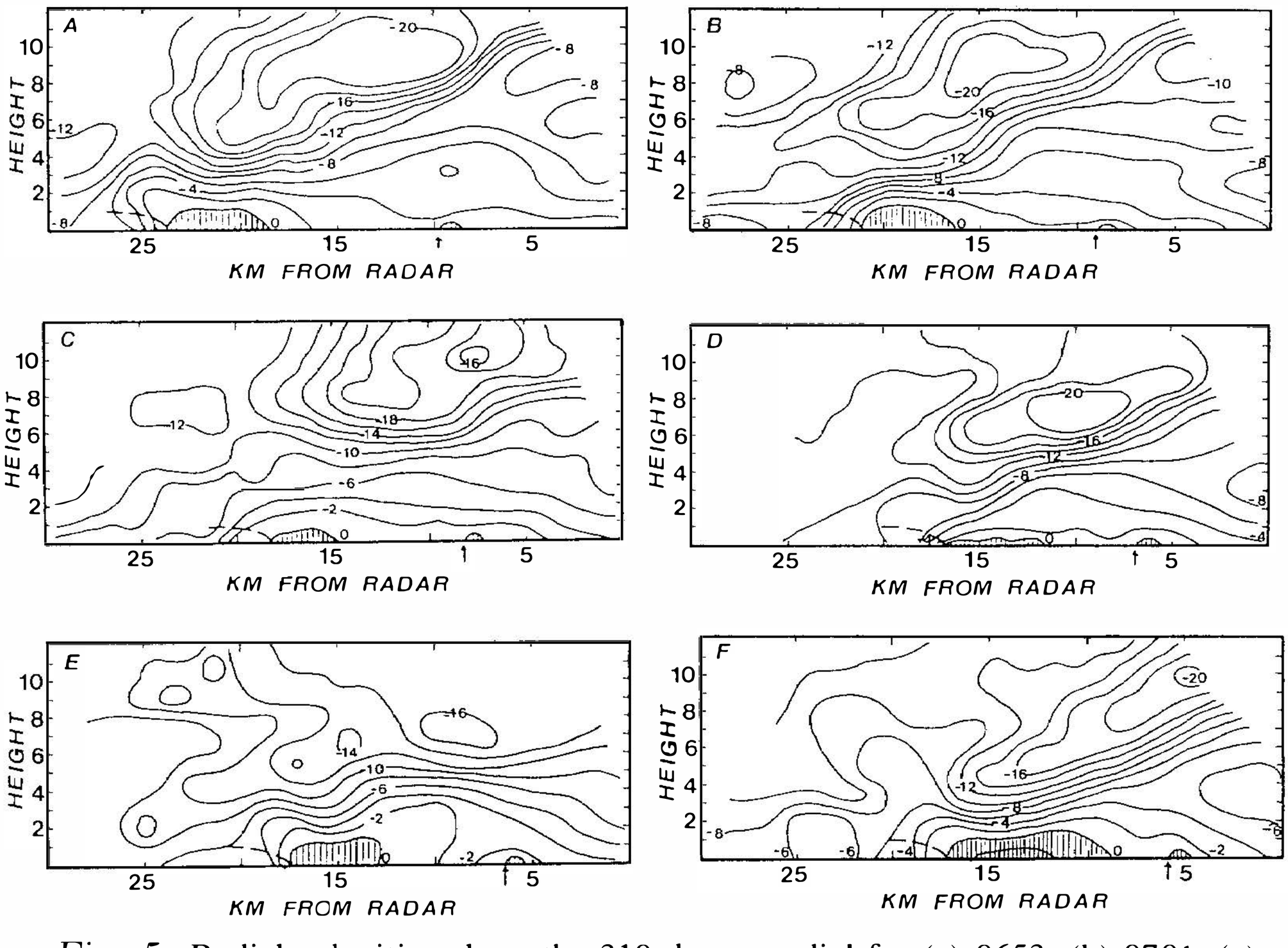

Fig. 5. Radial velocities along the 310 degree radial for (a) 0653, (b) 0701, (c) 0708, (d) 0716, (e) 0724, and (f) 0732 LST 25 June. The heavy dashed line and arrow indicate the position of the Mei-Yu front and gust front, respectively. The contour interval is 2 m/s with a positive (negative) value away from (toward) the radar. Distances are in kilometers from TOGA.

regions separated by the front, that is, the convective type in front and the stratiform type behind. Several cells were observed within the rainband with a maximum reflectivity near 45 dBZ. These reflectivity cores were confined to heights below 5.5 km. As noted in Lin *et al.* (1992), the warm-rain coalescence processes dominated in the IOP 13 since the freezing level was at 5.5 km.

As mentioned previously, a careful analysis of the radial velocity in the lowest layers can provide insight as to the mechanisms sustaining the long-lived system. The elongated downdraft in a widespread area ahead of the front produced a gust front characterized by negatively buoyant air which interacted with the high-θ_e air transported into the prefrontal region by the LLJ (Lin *et al.*, 1992). This would require a region of weak convergence co-located with the GF in the lowest layer. Figure 7 shows the radial velocity at 0.25 km along the 310 degree radial for the same time periods as in Figure 5 with the arrow denoting the approximate position of the GF as revealed by the single-Doppler analysis. Convergence may have been produced by speed convergence and not only by a change in sign within the two-dimensional frame of reference. This point is discussed in greater detail later. Examination of Figure 7 reveals that movement of the front (F) and the gust front (arrow) was relatively slow as the system gradually approached the coastline, which was in contrast to that observed

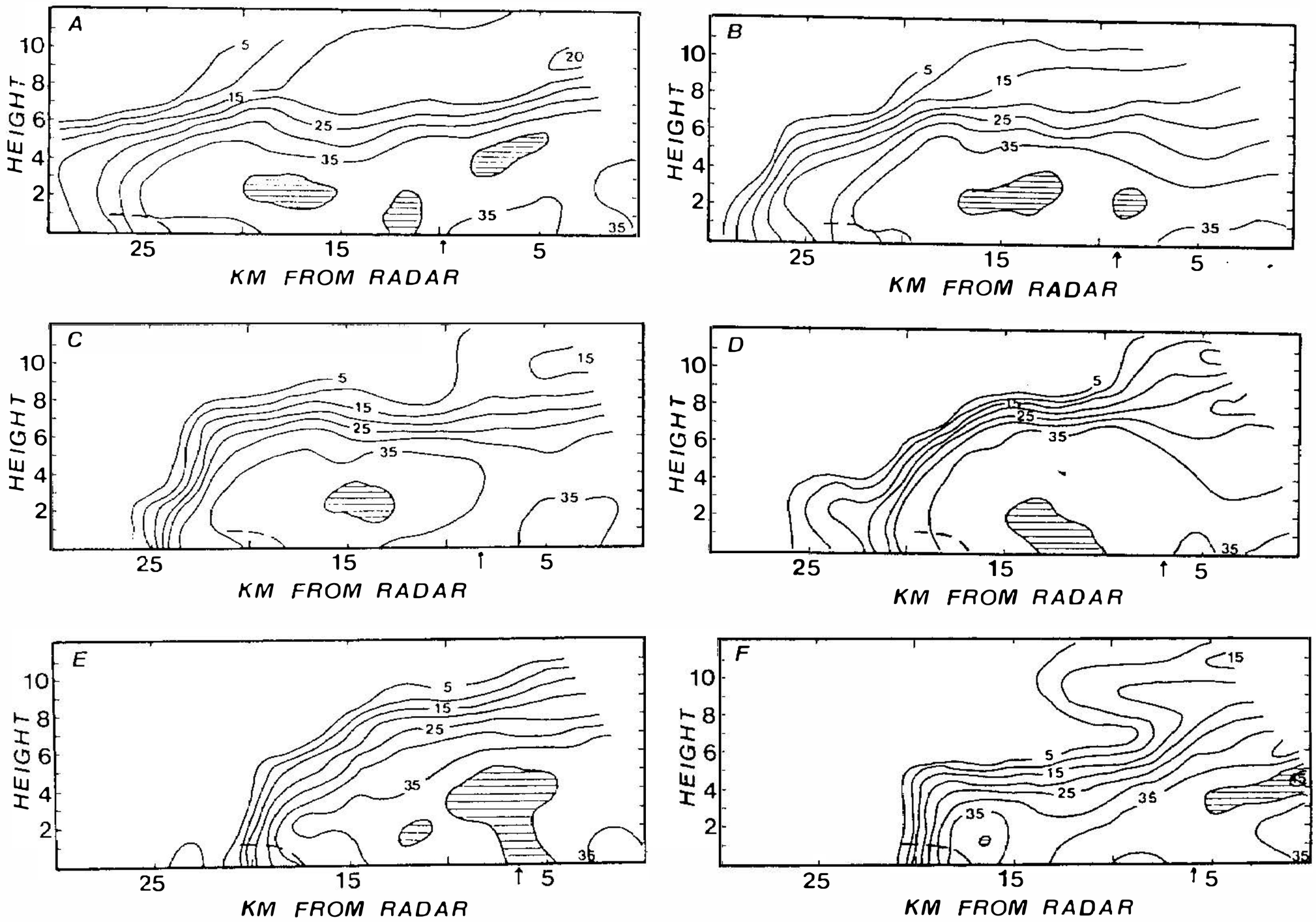

Fig. 6. As in Figure 5 except for reflectivity (Z). The contour interval is 5 dBZ. Areas with Z > 40 dBZ are hatched.

at earlier times when the system was located over northwestern Taiwan (Lin, 1993). These authors believe that the effect of the warm waters over the strait in late June continued to modify the cold air associated with the frontal system. This, in turn, affected the system movement as it traveled slowly down the central west coast (Lin *et al.*, 1993).

The values of the estimated horizontal convergences (divergences) along the 310 degree radial at 0.25 km, based on the radial velocity shear term in the radar viewing direction, are presented in Figure 8. The justification for employing this estimated convergence field to calculate vertical velocity in a direction nearly normal to the rainband can be found in Part II of this study. Units are in 10^{-3}/s with positive values (divergences) hatched. For comparison, the values of reflectivity in dBZ along the same radial are superimposed. In general, relatively weak convergence and strong reflectivity (30-40 dBZ) were observed at the GF (see the vertical arrow in Figure 8). This result is consistent with the rainband's structure since the GF was formed by cells at the leading edge of the rainband in the convective region ahead of the Mei-Yu front (Lin *et al.*, 1993). In contrast, the Mei-Yu front (F) was accompanied by relatively strong horizontal convergence (up to 4×10^{-3}/s) at the leading edge of the front (see the vertical dashed line in Figure 8) and weak reflectivity (Z < 20 dBZ) in the stratiform region behind the front. Between the two convergence zones at the F and GF, there was a broad area of divergence (hatched line) in the high reflectivity region with Z > 35 dBZ. This divergence zone near the surface was mainly caused by the horizontal spreading of descending air associated with the convective downdraft in the warm

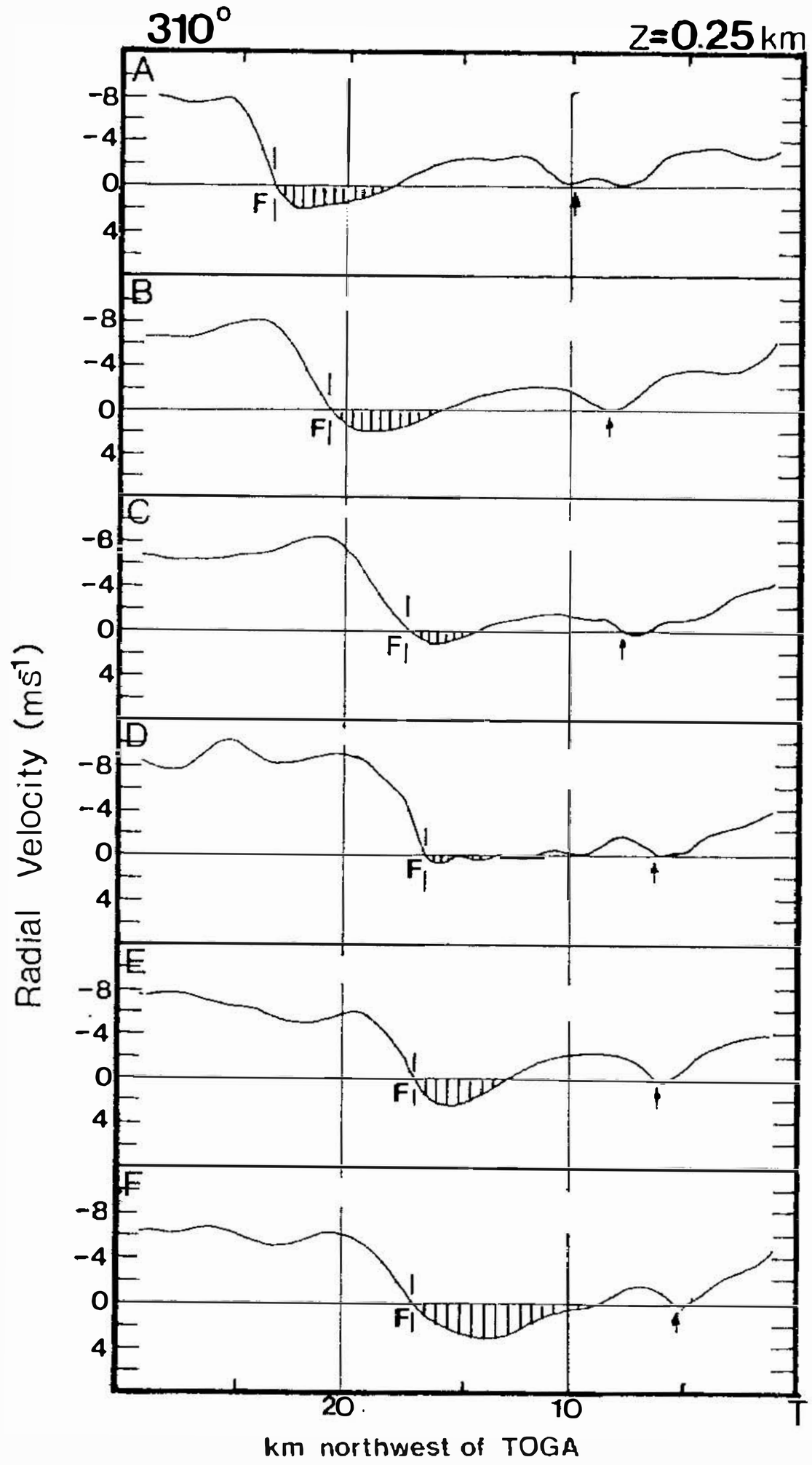

Fig. 7. Radial velocities along the 310 degree radial at 0.25 km above sea level for (a) 0653, (b) 0701, (c) 0708, (d) 0716, (e) 0724, and (f) 0732 LST 25 June.

sector mentioned earlier. This convective downdraft carried much cooler air with it from the middle and upper troposphere to the lower layer, resulting in a hydrostatically induced high pressure area near the surface (Lin *et al.*, 1993). This mesohigh, in turn, spread the cooler air horizontally in all directions. Portions of these cold horizontal outflows moved toward the southeast and northwest along the 310 degree radial, (see the negative and positive radial velocities,) respectively, in the area between the F and GF in Figure 5. These diverging outflows were largely responsible for maintaining the GF at the leading edge of the rainband and enhancing the low-level convergence at the front, respectively (Lin *et al.*, 1993). These findings clearly demonstrate that both the front and GF associated with the rainband can be properly identified with the single-Doppler analysis procedures described in this study. This point is further elaborated below.

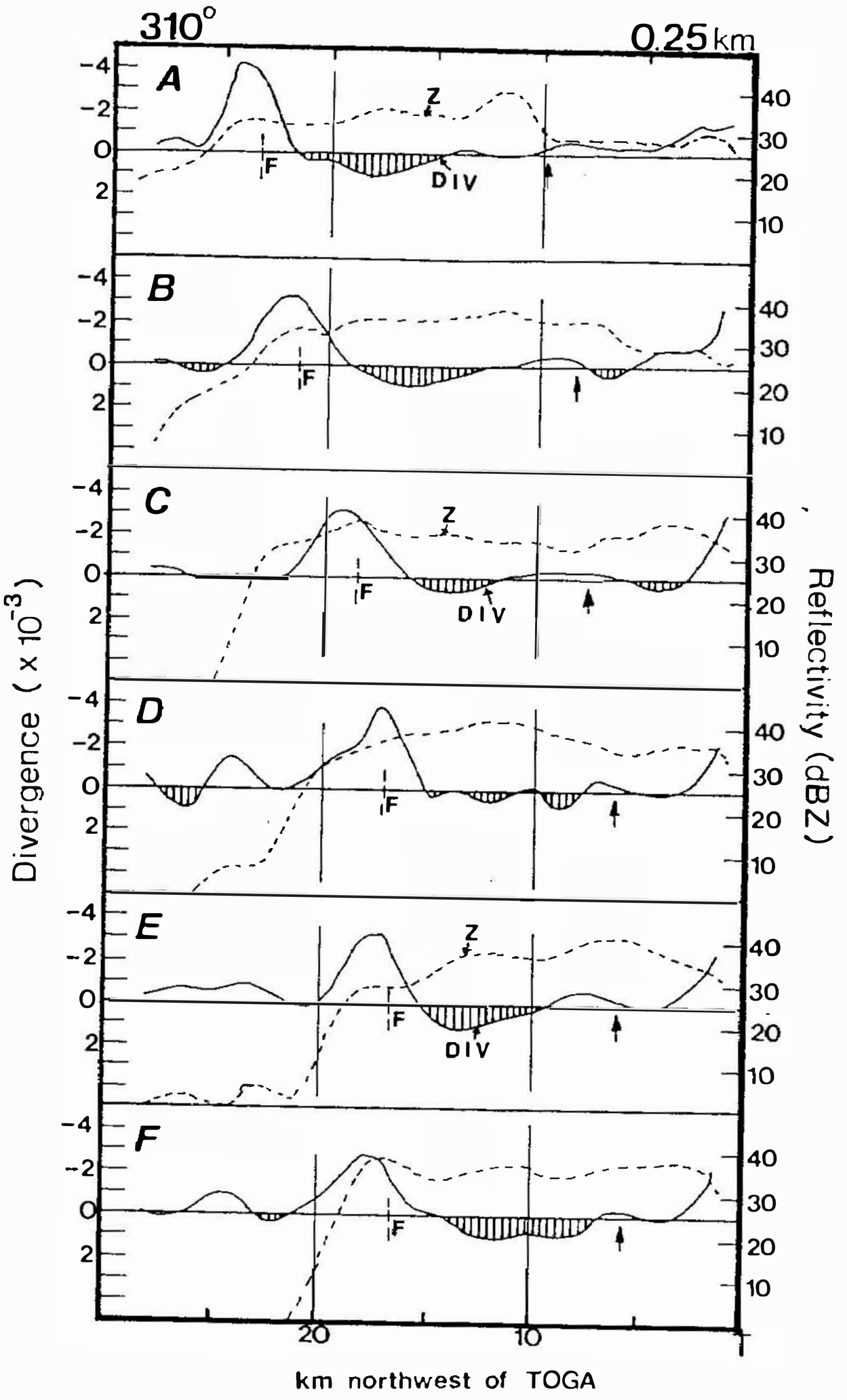

Fig. 8. As in Figure 7 except for convergence (solid line) and reflectivity (dashed line). Units for convergence and reflectivity are in 10^{-3}/s and dBZ, respectively.

3.7 Horizontal View of Doppler Measurements

Figure 9 displays the field of estimated horizontal convergence (divergence) at 0.25 km in the sector northwest of TOGA. This field was constructed using the information obtained at every kilometer along each of the nine radials between 290 and 330 degrees with the interval between any two 5 degrees. The sector is in the direction approximately normal to the front. Convergence is denoted by lined and hatched areas. The approximate positions of the front (heavy dashed line) and the GF (dotted line) at each analysis time determined from both the dual-Doppler analysis at 0653 and 0701 LST (Lin *et al.*, 1992 and Lin *et al.*, 1993) and single-Doppler analysis at 0708, 0716, 0724 and 0732 LST are superimposed.

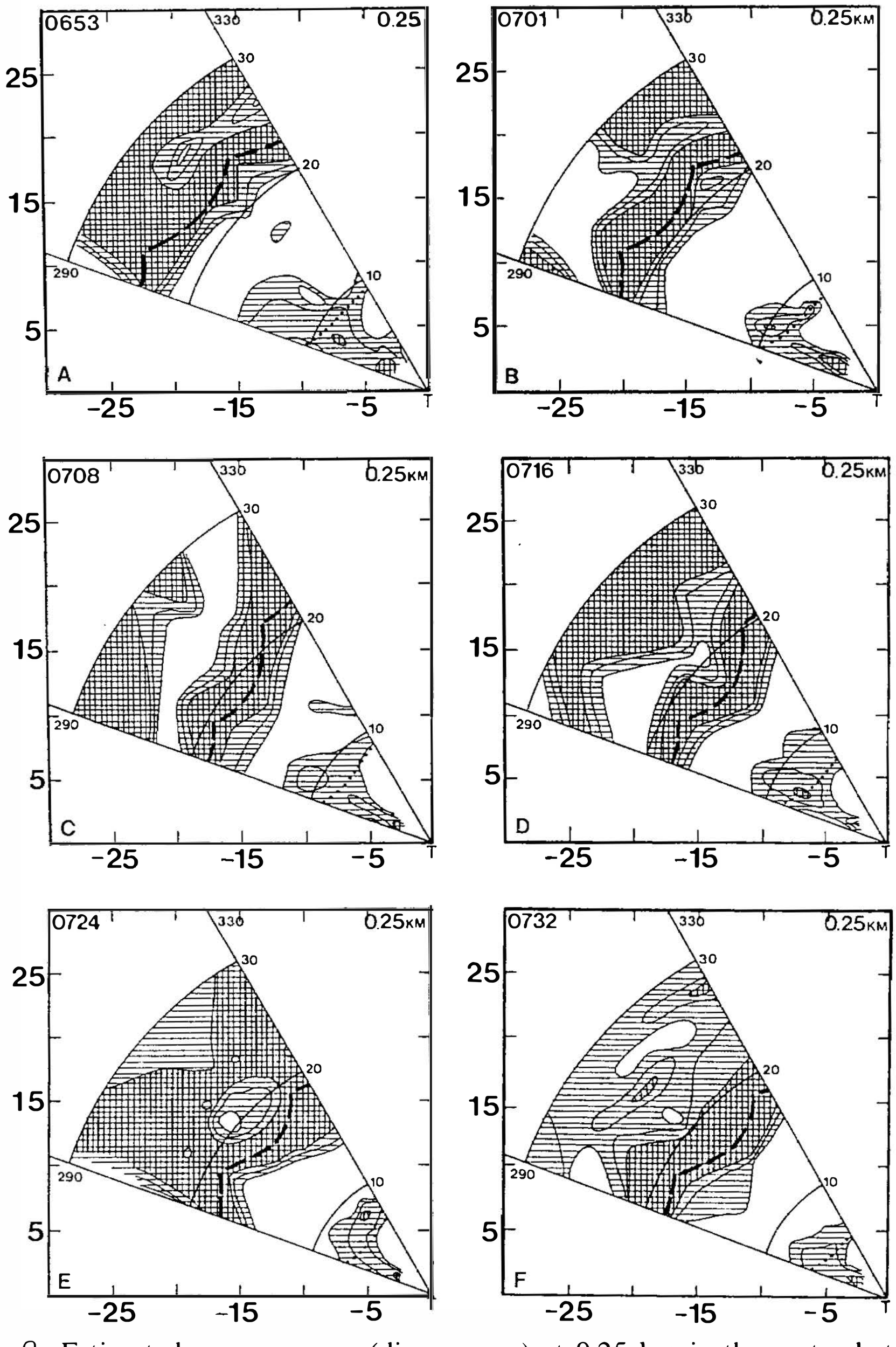

Fig. 9. Estimated convergences (divergences) at 0.25 km in the sector between 290 and 330 degrees for six times of analysis at (a) 0653, (b) 0701, (c) 0708, (d) 0716, (e) 0724, and (f) 0732 LST 25 June. The contour interval is 0.4×10^{-3}/s. Lined areas indicate weak convergence, while hatched areas denote relatively strong convergence (up to -5×10^{-3}/s). Range rings are every 10 km. The approximate positions of the F (heavy dashed line) and the GF (dotted line) are superimposed.

For comparison, the reflectivity from the CAPPI plot for 0.4 km at the same analysis times is shown in Figure 10. This reflectivity plot provides reference for cell locations in relation to the convergence field displayed in Figure 9. The contour interval is 10 dBZ beginning with 10 dBZ. Areas with reflectivity > 40 dBZ are shaded. Examination of Figures 9 and 10 reveals some interesting features. Of particular interest is an area of weak convergence with relatively strong reflectivity (35-40 dBZ) located near the TOGA radar, the area where the southeastward cold outflow collided with the southwest monsoon flow resulting in low-level convergence at the GF. As noted ealier, new convection developed along this GF and then merged with the older cells providing for the long-lived nature of this system (Lin *et al.*, 1992). Another zone of convergence (up to -5×10^{-3}) was found in a broad area 15-25 km northwest of TOGA. This is the area where the leading edge of the Mei-Yu front (heavy dashed line) was located. A striking feature seen in this area is a "kink" in the front. This "kink" is commonly observed in a typical cold front. Reflectivity was relatively strong at the front due to the frontal lifting of the warm, moist monsoon air in the warm sector. However, it became much weaker in a widespread area behind the front due to stratiform precipitation. It is to be noted that the divergence zone between the front and the GF was due to the downward motion associated with the convective downdraft over that region mentioned previously. These findings, as a whole, are in good agreement with those reported in the dual-Doppler study by Lin *et al.* (1992).

3.8 Discussion

The structural features of a cold front during the TAMEX IOP 8 were reported in the study by Trier *et al.* (1989) using single-Doppler radar data, upper air and surface observations. Results showed that the structure and propagation properties of a frontal system bore resemblance to those of a squall-line gust front in conjunction with the gravity/density current mechanism. The system was characterized by the moderate to high baroclinicity and abrupt wind shift associated with the front. According to Trier *et al.* (1989), this frontal system originated in a synoptic-scale deformation zone at mid-latitudes and then propagated toward the southeast at a moderate speed (8-9 m/s). Even though the amount of convective available potential energy (CAPE) was comparably small, strong frontal lifting was adequate to sustain a quasi-steady convective system at the leading edge of the front.

Unlike the case in the IOP 8, the frontal system in the IOP 13 traveled at a much slower speed in comparison with that estimated from the gravity/density mechanism. As explained in Lin *et al.* (1992), the presence of the CMR often divides a Mei-Yu front into two parts. The eastern part over the Pacific Ocean continues to travel at a (normal) rapid speed toward the southeast, while the western part (west and southwest of Taiwan) remains quasi-stationary, especially in the area close to the west coast of Taiwan. Based on the observations evidenc presented in this study, it was found that the system was traveling only at 2-3 m/s when it was located over the central west coast. The slow system speed was largely attributed to the presence of the CMR and the weak environmental northwesterly flow in the low layer behind the front.

As noted earlier, the leading edge of the rainband in the IOP 13 traveled at a more rapid speed when the system was located over the northwestern coast. At that time, the system was characterized by moderate baroclinicity. As the system continually traveled down the central west coast, its baroclinicity weakened considerably due to the effect of the warm waters over the strait (Trier *et al.* 1990). As a result, the movement of the gust front associated with

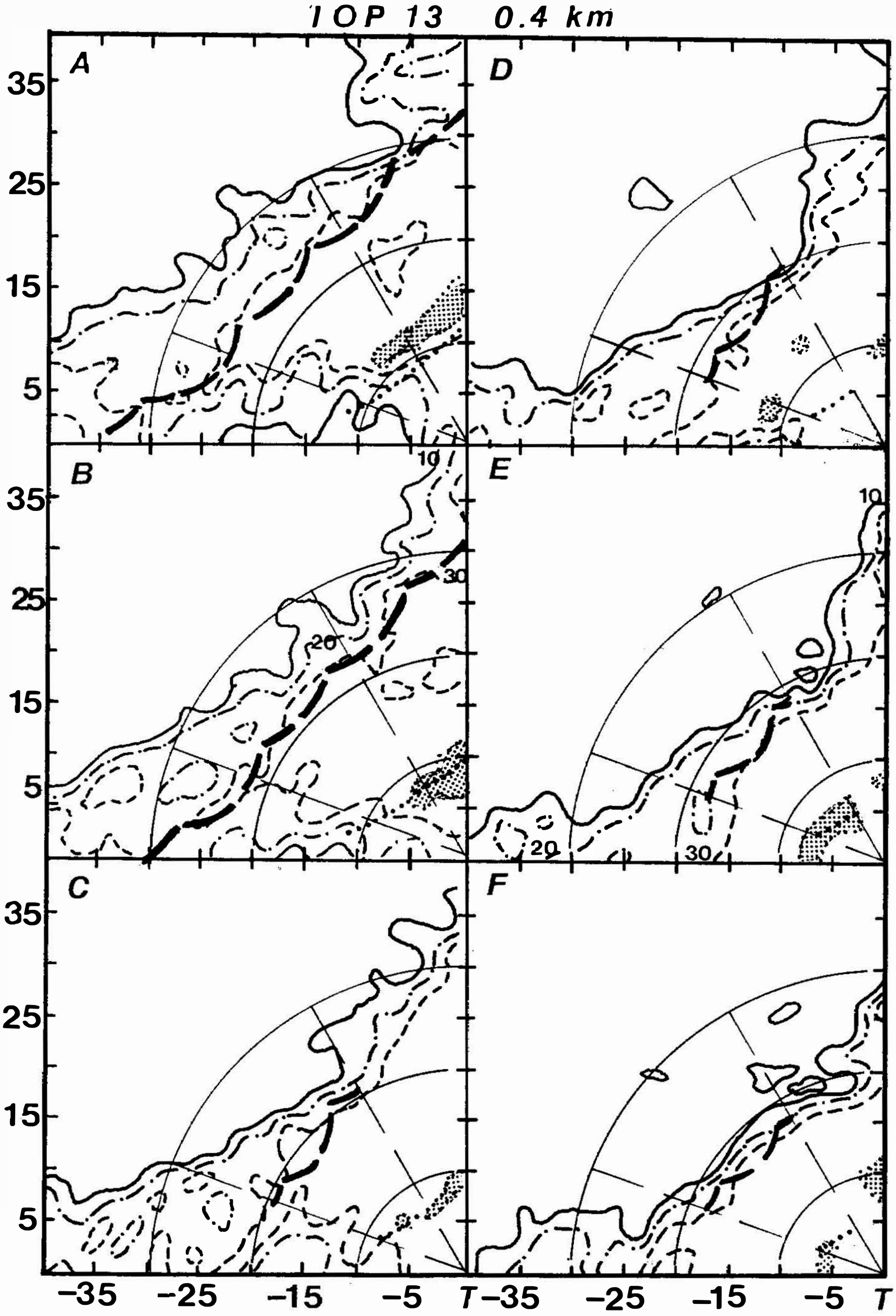

Fig. 10. Derived CAPPI scans for 0.4 km at (a) 0653, (b) 0701, (c) 0708, (d) 0716, (e) 0724, and (f) 0732 LST 25 June. The solid, dot-dash and dashed lines denote the 10, 20 and 30 dBZ reflectivity contours, respectively. Areas with reflectivity > 40 dBZ are shaded. Distances are in kilometers from TOGA (T).

the leading edge of the rainband slowed down drastically when compared to that over the northwestern coast (Lin, 1993). It is of interest to estimate the propagating speed based on the gravity/density current mechanism mentioned earlier.

A calculation of the density-current propagation speed similar to that of a gravity current driven squall-line gust front (Charba, 1974) was reported in studies by Carbone (1982), Trier *et al.* (1989), Lemaitre *et al.* (1989), etc. The von Karman (1940) approximation can be written as:

$$C = [K^2 g \Delta z \frac{(T_{v1} - T_{v2})}{T_{v2}}]^{0.5} \qquad (1)$$

where g is gravitational acceleration, δz is layer depth, T_v (K) is the virtual temperature and subscripts 1 and 2 refer to the lighter and denser masses, respectively. The value of k is chosen to be 0.84 (Lemaitre *et al.*, 1989), while the layer depth is 1 km (Lin *et al.*, 1992). With the aid of (1) and the surface observed temperatures prior to and after line passage, it was calculated that $c = 4.80\sqrt{\delta T}$ (m/s). Table 2 shows the relationship between the temperature difference δT and the propagation speed c obtained from (1). When the temperature difference before and after the gust-front passage was 1°C or greater, similar to that observed at several northern stations, the propagation speed was approximately 5 m/s or larger. On the other hand, when the temperature difference was less than 0.5°C, as reported at several west coast stations, the speed of the GF was reduced to only 2-3 m/s. These estimated speeds for gust-front propagation appear to agree well with those determined from the surface traces reported earlier in this study.

Table 2. The gravity-density propagation speed, similar to that of a gravity current driven squall-line gust front (Charba 1974), in relation to the temperature difference between the lighter (warmer) and denser (colder) masses.

$\delta(T)$	0.0	0.5	1.0	1.5	2.0	2.5	3.0
C (m/s)	0.0	3.4	4.8	5.9	6.8	7.6	8.3

4. SUMMARY AND CONCLUSIONS

The surface traces at 30-min intervals, obtained from the nine coastal stations, and conventional and Doppler radar measurements were used to further investigate the life cycle and cell evolution of the convective rainband during the IOP 13. Careful analyses have revealed several additional observations which support the conceptual model of this rainband, reported in the study by Lin et al. (1992) using two-volume scans of dual-Doppler data obtained from CP-4 and TOGA.

Results show that the rainband formed in the vicinity of the cold front when the system was located over the northwestern coast. As the rainband traveled slowly toward the south, it began to move away from the front as gust fronts were formed by cells at the system's leading edge. The density-current mechanism resulting from the cold outflows of convective cells in the lower layer was largely responsible for the more rapid movement of the rainband than the slow movement of the Mei-Yu front. The convective cells generated low-level cold outflows to the southeast of the front. Part of these cold outflows moved toward the southeast,

interacting with the strong moisture-rich southwest monsoon flow to form a gust front. At the same time, the southwestern portion of the front, located 50-60 km west of the coast, continued to lift moist air, generating new cells along the front. These new cells then traveled to the east at a speed of 6-7 m/s, following the low-level westerly flow over that region. The new cells eventually merged with the old (main) cells near the west coast, thereby prolonging the life span of the rainband. The slow movement of the front was mainly caused by the combined effects of the weak low-level northwesterly wind behind the front, the presence of the CMR and the warm waters over the Taiwan Strait in late June.

Acknowledgments The authors wish to express their appreciation to those scientists, technicians, and staff members who participated in the TAMEX project. They would like to thank the National Center for Atmospheric Research (NCAR) for providing Doppler data and technical assistance. Special thanks go to the National Science Council of the Republic of China and the National Science Foundation of the United States for supporting the field experiment. Discussions with Tai-Chi Chen Wang of National Central University, Ben Jou of National Taiwan University, and Komain Saisangthong of Saint Louis University are greatly appreciated. This work was supported by the Atmospheric Science Division, National Science Foundation, under NSF Grant ATM-9012135.

REFERENCES

Carbone, R., 1982: A severe frontal rainband. Part I: Storm-wide hydrodynamic structure. *J. Atmos. Sci.*, **39**, 258-279.

Charba, J., 1974: Application of gravity current model to analysis of squall-line gust front. *Mon. Wea. Rev.*, **102**, 140-156.

Jou, B. J., and S. M. Deng, 1990: Mesoscale characteristics of Mei-Yu front: A TAMEX case study. Proc., Workshop on TAMEX Scientific Results, Boulder, NCAR, 150-157.

Lemaitre, Y., G. Scialom, and P. Amayenc, 1989: A cold frontal rainband observed during the LANDES-FRONTS 84 Experiment: Mesoscale and small-scale structure inferred from dual-Doppler radar analysis. *J. Atmos. Sci.*, **46**, 2215-2235.

Li, J., Y. L. Chen, and W. C. Lee, 1995: Analysis of a heavy rainfall event during TAMEX. Proc., Int'l Workshop on Heavy Rainfall in East Asia, 27-29 March, Seoul, Korea, 82-89.

Lin, Y. J., R. W. Pasken, and H. W. Chang, 1992: The structure of a subtropical prefrontal convective rainband. Part I: Mesoscale kinematic structure determined from dual-Doppler measurements. *Mon. Wea. Rev.*, **120**, 1816-1836.

Lin, Y. J., H. W. Chang, and R. W Pasken, 1993: The structure of a subtropical prefrontal convective rainband. Part II: Dynamic and thermodynamic structures and momentum budgets. *Mon. Wea. Rev.*, **121**, 1671-1687.

Lin, Y. J., 1993: Structural features of a subtropical squall line determined from dual-Doppler data (invited paper). Proc., Int'l Workshop on Mesoscale Research and TAMEX Program Review, Taipei, Taiwan, 13-27.

Mannouji, N., and K. Kurihara, 1990: A numerical experiment of TAMEX IOP #13 by the spectral limited area model of JMA. Proc., Workshop on TAMEX Scientific Results, 24-26 September, Boulder, 121-126.

Pasken, R. W., and Y. J. Lin, 1991: Mesoscale structure of a Mei-Yu front during IOP-13 based on single Doppler measurements. Proc., Int'l Conference on Mesoscale Meteorology and TAMEX, Taipei, Taiwan, 3-6 December, 76-84.

Trier, S. B., D. B. Parsons and T. J. Matejka, 1989: Observations of a cold front during TAMEX. Proc., Workshop on TAMEX Preliminary Scientific Results, 22-30 June, Taipei, Taiwan, 186-195.

Trier, S. B., D. B. Parsons, and T. J. Matejka, 1990: Observations of a subtropical cold front in a region of complex terrain. *Mon. Wea. Rev.*, **118**, 2449-2470.

Von Karman, T., 1940: The engineer grapples with nonlinear problems. *Bull. Am. Math. Soc.*, **46**, 615-623.